reactions

MDPI

Article

Effect of Pre-Treatment Conditions on the Activity and Selectivity of Cobalt-Based Catalysts for CO Hydrogenation

Nothando C. Shiba, Xinying Liu, Diane Hildebrandt and Yali Yao *

Institute for Development of Energy for African Sustainability (IDEAS), College of Science, Engineering and Technology, University of South Africa, Private Bag X6, Johannesburg 1710, South Africa; shibacynthia@gmail.com (N.C.S.); Liux@unisa.ac.za (X.L.); hilded@unisa.ac.za (D.H.)
* Correspondence: yaoy@unisa.ac.za

Abstract: We investigated the effect of pre-treatment conditions on the activity and selectivity of cobalt catalysts for Fischer–Tropsch synthesis (FTS) by varying both the reduction atmosphere and the reduction temperature. Catalysts supported on SiO_2, Al_2O_3, and TiO_2, prepared via incipient wetness impregnation, were evaluated, and activation temperatures in the range 250–350 °C were considered. Activation with syngas led to a better product selectivity (low CH_4, high selectivity to liquid hydrocarbons, and low paraffin to olefin ratio (P/O)) than the catalysts reduced in H_2 at lower activation temperatures. The Co_xC species suppressed the hydrogenation reaction, and it is hypothesised that this resulted in the high selectivity of olefins observed for the syngas pre-treated catalysts. On the basis of the experimental results, we postulated that a synergistic effect between Co^0 and Co_xC promotes the production of the long chain hydrocarbons and suppresses the formation of CH_4. In addition, for systems aimed at producing lower olefins, syngas activation is recommended, and for the FTS plants that focus on maximising the production of higher molecular weight products, H_2 activation might be considered. These results provide insights for the future FTS catalyst design and for target product-driven operations.

Keywords: CO hydrogenation; cobalt carbides; Fischer–Tropsch synthesis; pre-treatment; reduction

Citation: Shiba, N.C.; Liu, X.; Hildebrandt, D.; Yao, Y. Effect of Pre-Treatment Conditions on the Activity and Selectivity of Cobalt-Based Catalysts for CO Hydrogenation. *Reactions* **2021**, *2*, 258–274. https://doi.org/10.3390/reactions2030016

Academic Editors: Dmitry Yu. Murzin and Wenping Ma

Received: 27 April 2021
Accepted: 30 July 2021
Published: 6 August 2021

1. Introduction

Fischer–Tropsch synthesis (FTS) is a structure-sensitive reaction that converts syngas derived from natural gas, coal, and biomass to valuable chemicals and synthetic fuels over a metal-based catalyst [1]. Cobalt (Co) catalysts have attracted more attention in the recent years due to their high intrinsic hydrogenation activity, selectivity towards liquid hydrocarbons, and lower water gas shift (WGS) activity than iron and lower costs compared to noble metals [2,3]. Currently silica (SiO_2), alumina (Al_2O_3), and titania (TiO_2) are used for commercial FTS operations [4].

The hydrogenation activity of the cobalt metal (Co), which is recognised as the active phase, is highly dependent on its structure. Co particles that are hexagonally packed (hcp) are found to be more active than the face-centred cubic (fcc) structure [5,6]. Evidence from previous studies suggests that the Co particle size is influenced by the support pore size [7–9]. Borg [10] studied the dependency of the Co particle size on the Al_2O_3-support pore diameter and found that: (i) large Co particles were formed in the large pores and smaller ones formed in the narrow pores, (ii) the degree of reduction increased with the pore size, and (iii) the C_{5+} (the long chain hydrocarbons with carbon numbers equal or higher than 5) selectivity also increased with the pore size.

In some cases, the interaction between these supports and the metal can be too strong, which may leave a fraction of the cobalt chemically inactive after reduction. For example, Jacobs et al. [11] reported a lower degree of reduction for Al_2O_3- and TiO_2-supported catalysts due to high metal–support interactions compared to the SiO_2-support. Strong metal–metal oxide interactions have been demonstrated to play an important role in the

reactivity of alumina-supported catalysts. A specific feature in these catalysts is incomplete reduction and possibly the insertion of Co ions into the alumina lattice to form spinel structures, and as a result, the catalysts exhibit low reducibility and FT activity [12]. To overcome this issue, several strategies such as the modification of the support to minimise deleterious support metal interactions have been put forward. Soled et al. [13] demonstrated that the use of silicon substitutions in the TiO_2 lattice and the treatment of the TiO_2 support using an irreducible oxide ZrO_2 can inhibit the formation of Co–support interactions and thereby enhance the reducibility of the catalysts. Other strategies to limit the solid-state chemistry interactions between Co and the support include the use of neutral supports such as carbon nanofibers [14] and small amounts of noble metal promoters [15].

Significant efforts have been devoted to enhancing the catalytic activity of FTS catalysts and to reducing the costs of the FTS process. Hydrogen (H_2) is used to activate the Co_3O_4 species in freshly prepared catalysts to active metallic Co. A few studies documented the use of syngas as an alternative reducing agent to H_2 [16–18]. The general consensus is that syngas reduction promotes the formation of cobalt carbides (Co_xC, x = 2, 3), which transform back to metallic Co(hcp) under normal FT operating conditions, thus improving the FT activity [18], or that the inactive Co_xC blocks the Co metal active sites, leading to catalyst deactivation [19]. De la Pena O'Shea et al. [16] achieved a significantly higher activity (90% CO conversion) with a Co/SiO_2 catalyst pre-treated in syngas compared to either H_2 or CO reduction. The improvement in activity was attributed to the increase in the number of Co active sites (high metal dispersion). The presence of Co_2C during FTS has been confirmed by Claeys et al. [20] and reported to act as a methanation site [21,22]. While the role of Co_2C is widely debated in FTS, the presence of Co_2C nanoprisms increase the selectivity towards alcohols and olefins [19,23].

Syngas reduction is conducted at relatively low temperatures (<280 °C) to avoid catalyst coking resulting from the degradation of liquid products, and to limit the deposition of inactive surface carbon via the Boudouard reaction [18,24]. Graphitic carbon has been reported to strongly suppress CH_4 formation; however, it cannot be removed from the surface, thus it blocks the Co active sites and results in catalyst deactivation [24]. De la Pena O'Shea [16] reported that no graphitic carbon was observed after the syngas treatment at 500 °C due to the simultaneous presence of H_2 and CO, which minimises the formation of carbon. Reducing the catalyst at a low temperature with syngas still produces a fraction of CoO, which is believed to be inactive in FTS [25], and to catalyse the WSG reaction [26]. In our earlier work, we reported that the intimate contact between CoO and Co metal as well as formation of Co–CoO interfaces under FT reaction conditions catalyses the FT reaction for a SiO_2-supported catalyst pre-treated in H_2 at 250 °C [27].

Although there is a large body of work on the effect of the reduction temperature including the support characteristics on various Co-based catalysts reduced under H_2, not as much attention has been paid to determine how temperature and support identity influences the reduction of Co species under syngas reduction. As H_2 is an expensive gas, the use of syngas, as both reaction and reducing agents, at lower reduction temperatures can potentially cut-down the start-up and running costs of an FT process. Here, we report on the activity and selectivity of Co catalysts supported on TiO_2 and Al_2O_3, reduced at two temperatures (250, 350 °C) under two reductive agents (H_2, syngas), per catalyst, to compare their influence on CO hydrogenation.

2. Experimental Set-Up

2.1. Catalyst Preparation

In this work, three kinds of supports, TiO_2, SiO_2, and Al_2O_3 were used for the preparation of the 15% Co/support catalysts. The catalysts were prepared via incipient wetness impregnation of cobalt nitrate solution ($Co(NO_3)_2{\cdot}6H_2O$) onto these three kinds of supports. The chemicals used were outsourced from Sigma-Aldrich (St. Louis, MO, USA). Catalysts were dried at room temperature overnight, followed by mild drying at 40 °C for

3 h and calcination at 350 °C for 8 h. For, the detailed preparation procedure, please refer to our earlier publication [27].

2.2. Catalyst Characterisation

Brunauer–Emmet–Teller (BET) experiments were conducted on the fresh catalysts prior to reduction or reaction to determine the sample surface area and pore size. BET experiments followed the usual procedure. The sample was firstly subjected to a degassing chamber at 200 °C for 6 h, and treatment was performed at a relative pressure of 0.99 (P_a/P_0 = 0.99, where P_a is the actual gas pressure and P_0 is the vapor pressure of the adsorbing gas) to obtain the pore volume and −196 °C to obtain the surface area and porosity by nitrogen physisorption. Furthermore, the Barrett–Joyner–Halenda (BJH) method was used to obtain the pore sizes from the desorption branches on the isotherms.

The morphology of the catalysts was characterised by transmission electron microscopy (TEM). The samples for TEM studies were prepared by ultrasonic dispersion of the catalysts in ethanol, and the suspensions were added dropwise onto a copper grid. The TEM investigations were carried out using a JEOL-JEM-100CX II (100 kV) transmission electron microscope equipped with a NARON energy-dispersive spectrometer and a germanium detector.

X-ray diffraction (XRD) studies were performed using a Philips PW 1710 spectrometer with monochromatic Cu-Kα radiation to determine the catalyst particle size and crystalline structures. The measurements were made on calcined catalysts and the average Co_3O_4 particle size was calculated from the most intense peak, with the use of Scherrer formula [6], for each catalyst.

The reduction behaviour and the interaction between the active phase and the support of each catalyst were examined using the temperature programmed reduction (TPR) technique. The TPR experiments were carried out with a thermal conductivity detector (TCD) to determine the hydrogen consumption. The catalyst (500 mg) was placed in a quartz tubular reactor fitted with a thermocouple for continuous temperature measurements. The reactor was heated with a furnaced designed for the TPR machine, at a ramping rate of 10 °C/min, under a mixture of 5 vol % H_2 in an air flow of 30 cm^3/min.

2.3. Reduction and Reaction Procedures and Data Analysis

Three fixed bed reactors with the same size (ID = 8 mm) were used in this study. One gram of Co/SiO_2, Co/Al_2O_3, and Co/TiO_2 catalysts was loaded into the three respective reactors. The three catalysts followed the same activation procedures: to reduce in a flow of either H_2 or syngas (H_2/CO ratio of 2) at two different temperatures, namely, 250 °C and 350 °C, and atmosphere pressure. After catalyst reduction, the catalysts were cooled to 180 °C. Thereafter, the same syngas used for catalyst reduction was introduced for FTS. The catalyst reactivity and product distribution were evaluated at 20 bar, 210 °C, and 60 mL/min with syngas.

The tail gases from the three reactors were monitored and analysed by an online GC (Agilent 7890B): the hydrocarbon products were analysed by a flame ionisation detector (FID), whist the other gases (H_2, CO, N_2, and CO_2) were analysed by two TCDs.

3. Results

3.1. Characteristics

Table 1 lists the physical properties of the catalysts. It shows that the Al_2O_3-supported catalyst had a larger pore size and a larger particle size than the catalysts supported on TiO_2 and SiO_2. For further details on the catalyst physical properties, please refer to our previous publications [27].

The crystal morphology of the catalysts is illustrated in Figure 1, determined via TEM. In the cross sections, the visible darker dense areas represent Co_3O_4 particles, and the lighter areas correspond to the support. The Co_3O_4 particles seemed to be more highly dispersed on the TiO_2-support followed by SiO_2-support then the Al_2O_3-support. This

might have been due to the smaller TiO_2-support particles that are observed in Figure 1. The large Co_3O_4 particles observed on the alumina support suggest that the support had a wider pore, thus distributing bigger particles than TiO_2 and SiO_2. The Co_3O_4 particles on the Al_2O_3- and SiO_2-supports seemed to be spherical shape, whilst on the TiO_2, the cobalt particles assumed the shape of the TiO_2-support particles, in this case cubic/rhombus-shaped.

Table 1. Physical properties of the catalysts and reactor used in this work.

Catalyst	15% Co/SiO_2	15% Co/Al_2O_3	15% Co/TiO_2
Catalyst BET pore size (nm)	6.8	43.1	38.7
Catalyst BET surface area (nm)	407.0	115.8	88.4
TEM average particle size (nm)	26	38	28
XRD crystallise size (nm)	17.0	33.0	21.5
Reactor		Fixed bed reactor	
Reactor diameter (mm)	0.8	0.8	0.8
Catalyst weight loaded into the reactor (g)	1	1	1

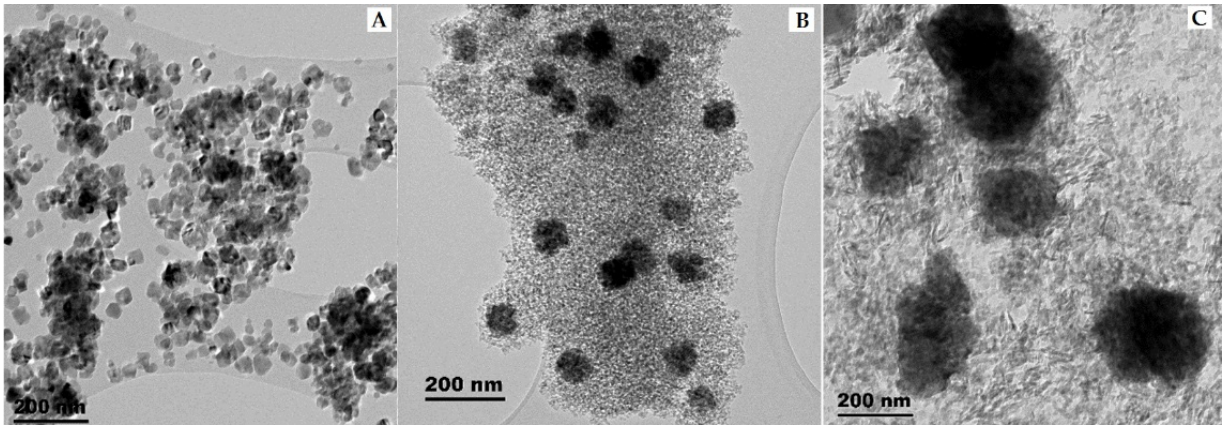

Figure 1. TEM micrograph images of a freshly calcined catalyst: (**A**) Co/TiO_2, (**B**) Co/SiO_2, and (**C**) Co/Al_2O_3.

The XRD patterns for the model catalysts (Co/TiO_2, Co/SiO_2, Co/Al_2O_3) are presented in Figure 2. XRD characteristics of Co_3O_4 were detected for all the calcined catalysts with Co/TiO_2 and Co/Al_2O_3, showing distinctive Co_3O_4 crystalline features, marked with a black circle (see Figure 2). The Co/SiO_2 diffractogram showed considerably broad features, which suggests that the silica support is likely amorphous, and contains smaller Co_3O_4 nanoparticles. The average Co_3O_4 crystallite size (Table 1) was calculated from the Scherrer equation [6]. The Co_3O_4 crystallite size varied slightly as a function of the pore size, with Co/Al_2O_3 showing the biggest size (33.0 nm), owing to its large pore size, followed by Co/TiO_2 (21.5 nm) and then lastly Co/SiO_2 (17.0 nm).

The TPR reduction profiles presented in Figure 3 for the three kinds of catalysts showed two reduction peaks, which were similar to those observed for bulk Co_3O_4 oxide. These profiles point to a two-step reduction process: the first one of low intensity started at approximately 200 °C and overlapped with the more intense second peak whose maximum occurred at about 300 °C for Co/TiO_2 and Co/SiO_2 catalysts, and for Co/Al_2O_3, the peak started around 300 °C and the second peak emerged at around 450 °C. Other than the fact that the second reduction peak for the Al_2O_3-supported catalyst emerged at a higher temperature than the second peak on the TiO_2- or SiO_2-supported catalysts, it also extended its shoulder to a higher magnitude, in this case 700 °C. Therefore, the reduction process of Co_3O_4 can be described by the reduction of Co^{3+} ions present in the spinel structure of a fresh catalyst into Co^{2+} with subsequent structural change to CoO, followed by the

reduction of Co^{2+} ions to Co^0 metal. The results observed over the Al_2O_3-supported sample suggests that the catalyst supported on Al_2O_3 is harder to reduce than the one supported by TiO_2 or SiO_2, which may have been due to strong metal–support interactions, which is in line with the literature [11,12].

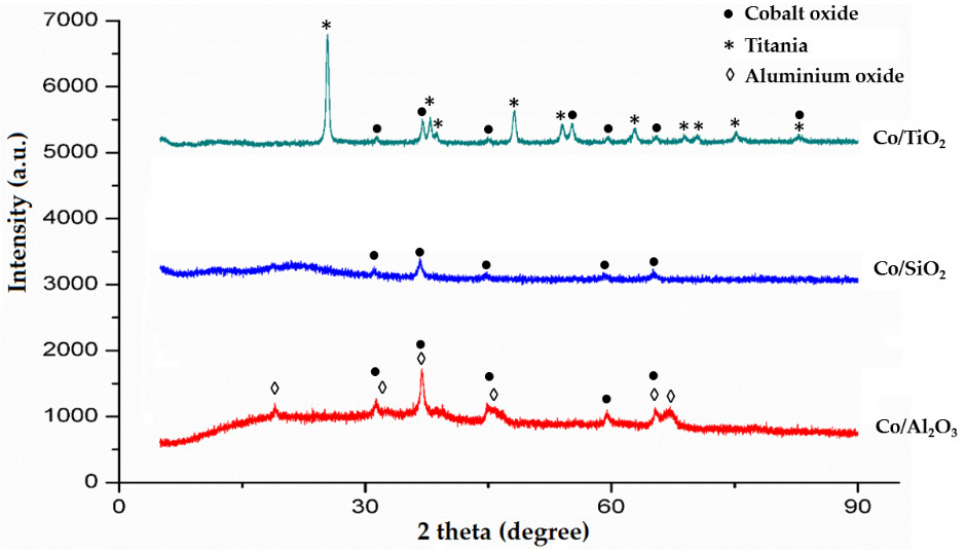

Figure 2. XRD patterns of freshly calcined Co/TiO_2, Co/Al_2O_3, and Co/SiO_2 catalysts.

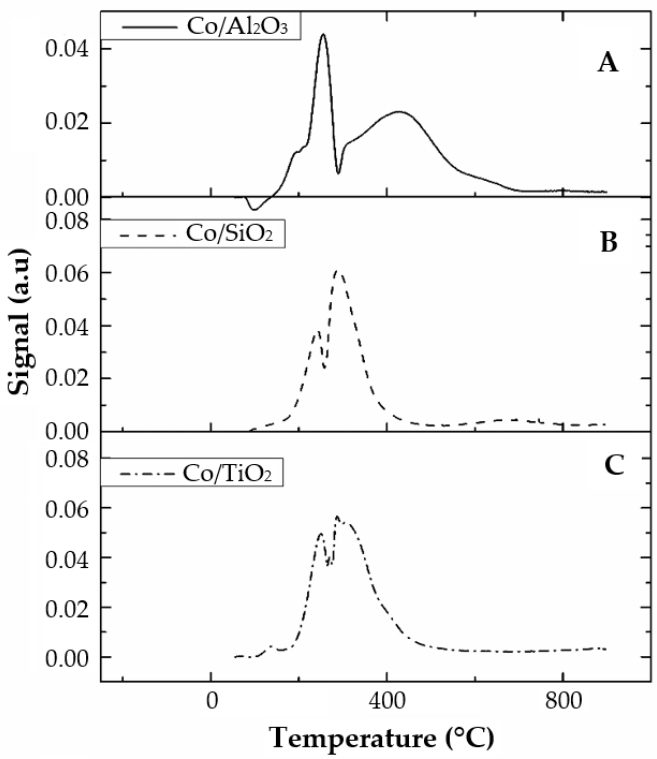

Figure 3. TPR reduction profiles for (**A**) Co/Al_2O_3 (solid line), (**B**) Co/SiO_2 (dashed line), and (**C**) Co/TiO_2 (dashed and dotted line). Reproduced from Shiba et al. [27] with permission from Elsevier, license number 5053041467597.

Furthermore, a higher reduction temperature was required for the reduction of the Al_2O_3-supported catalyst compared to TiO_2- and SiO_2-supported catalysts, as observed from of the reduction profiles (Figure 3), which might have been due to the fact that the

cobalt particles diffused into the Al_2O_3 lattice and formed the irreducible compounds, such as aluminates.

3.2. Catalyst Activity and Selectivity

3.2.1. Reaction Rate

The Fischer–Tropsch (FT) activity and selectivity of the supported cobalt catalysts is illustrated in Figures 4–10. The catalysts pre-treated in H_2 exhibited higher CO reaction rates compared to the samples reduced in syngas, at all reduction temperatures (see Figure 4). For the syngas pre-treatment, the CO reaction rates were found to be higher at a higher reduction temperature (350 °C) for all the samples. Similar results to the syngas pre-treatment were observed, where higher CO reaction rates were achieved at a higher reduction temperature for all the three catalysts reduced in H_2 (except for the SiO_2 catalyst reduced in H_2 at 250 °C).

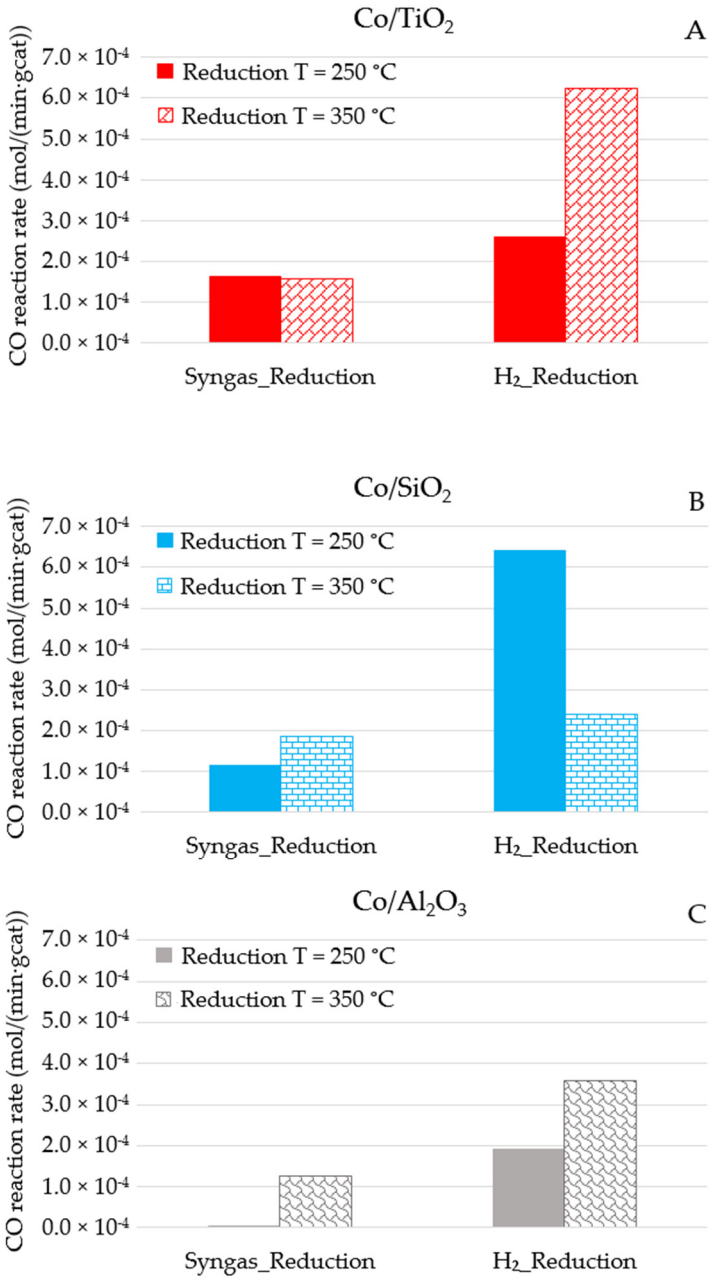

Figure 4. CO reaction rate as a function of reducing agent and temperature: (**A**) for Co/TiO_2, (**B**) for Co/SiO_2, and (**C**) for Co/Al_2O_3. Reaction conditions: 20 bar, 60 mL/min, and 210 °C.

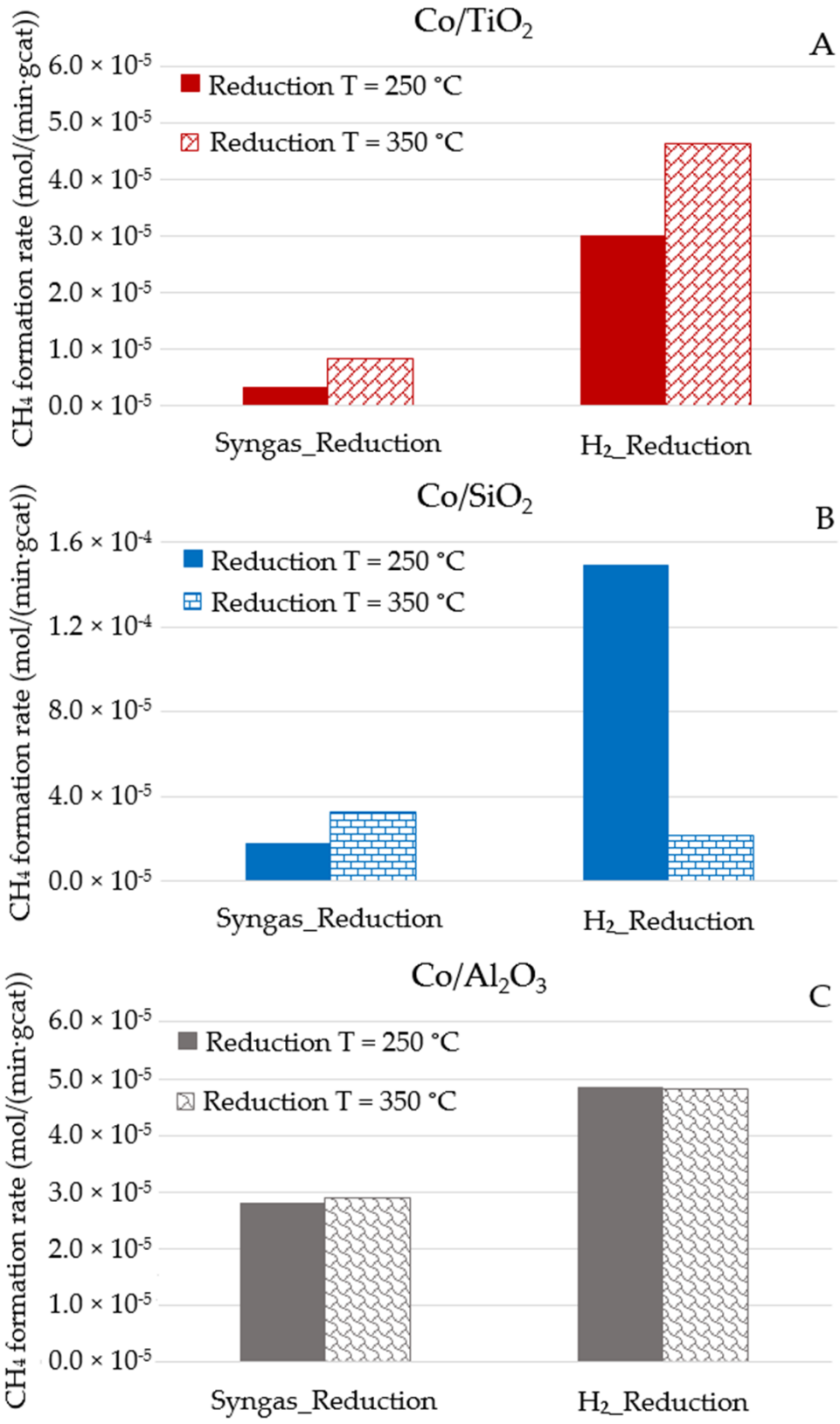

Figure 5. CH_4 formation rate as a function of reducing agent and temperature: (**A**) for Co/TiO_2, (**B**) for Co/SiO_2, and (**C**) for Co/Al_2O_3. Reaction conditions: 20 bar, 60 mL/min, and 210 °C.

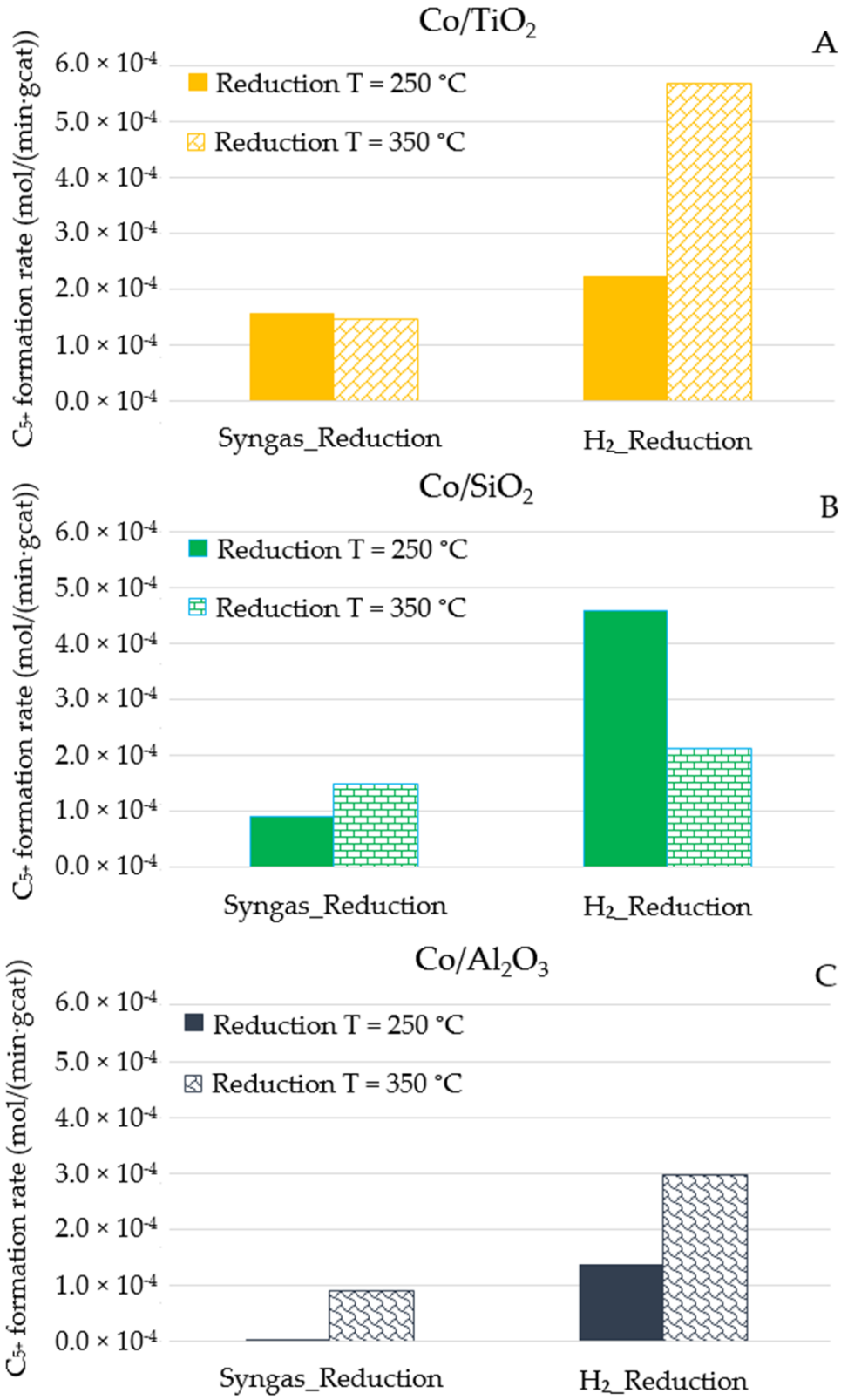

Figure 6. C_{5+} formation rate as a function of reducing agent and temperature: (**A**) for Co/TiO_2, (**B**) for Co/SiO_2, and (**C**) for Co/Al_2O_3. Reaction conditions: 20 bar, 60 mL/min, and 210 °C.

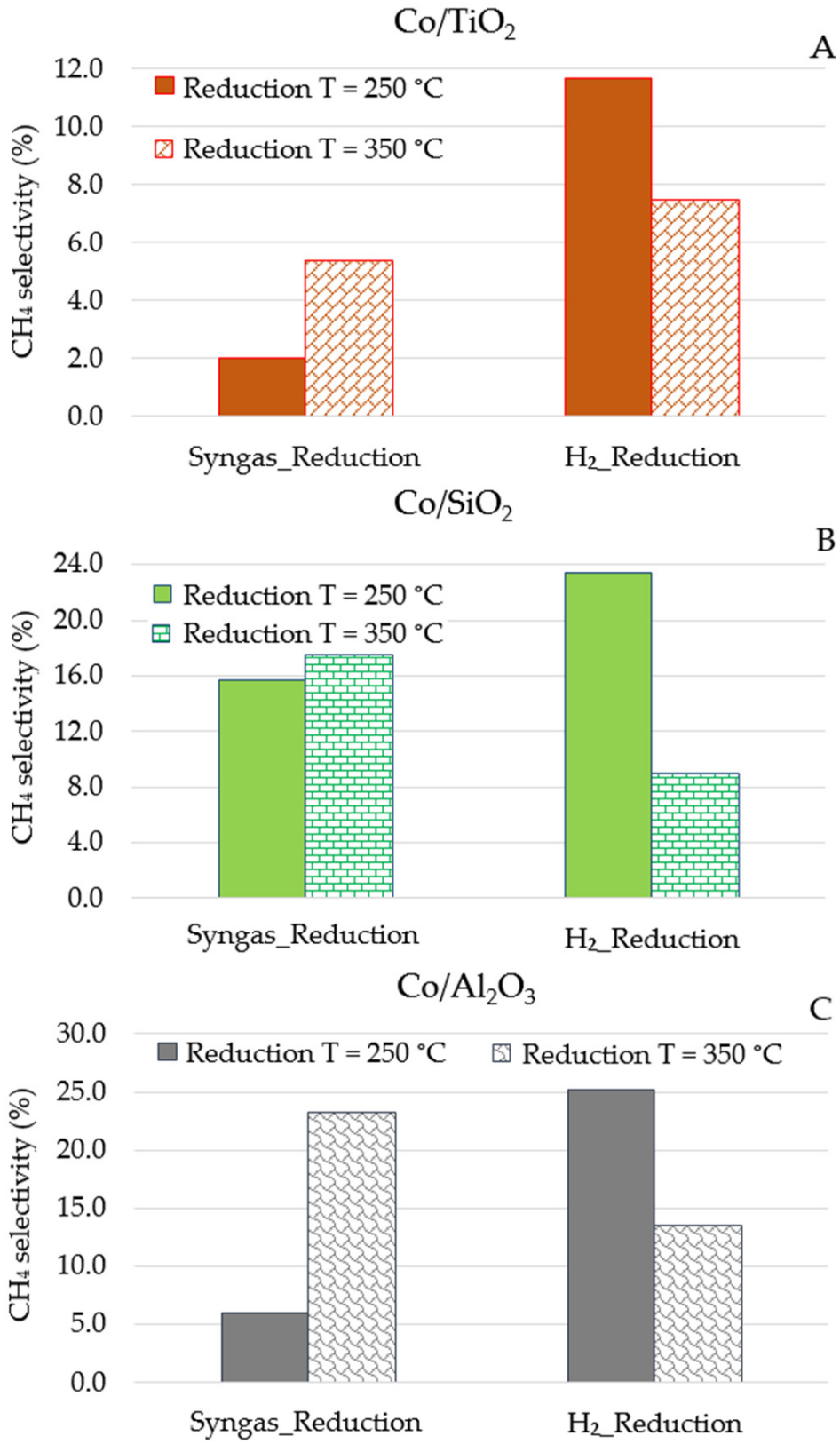

Figure 7. The selectivity of CH_4 as a function of reducing agent and temperature: (**A**) for Co/TiO_2, (**B**) for Co/SiO_2, and (**C**) for Co/Al_2O_3. Reaction conditions: 20 bar, 60 mL/min, and 210 °C.

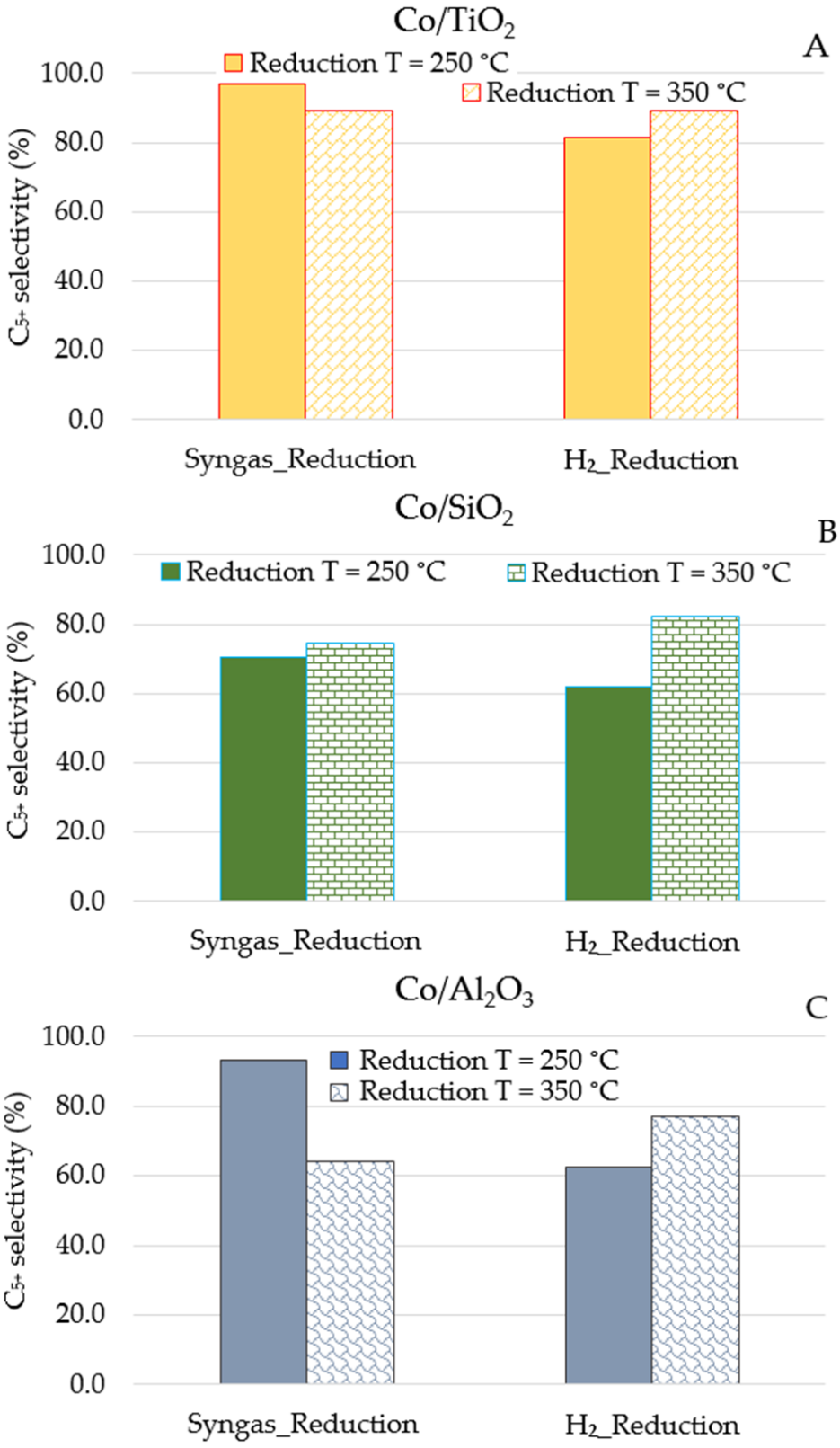

Figure 8. The selectivity of C_{5+} as a function of reducing agent and temperature: (**A**) for Co/TiO_2, (**B**) for Co/SiO_2, and (**C**) for Co/Al_2O_3. Reaction conditions: 20 bar, 60 mL/min, and 210 °C.

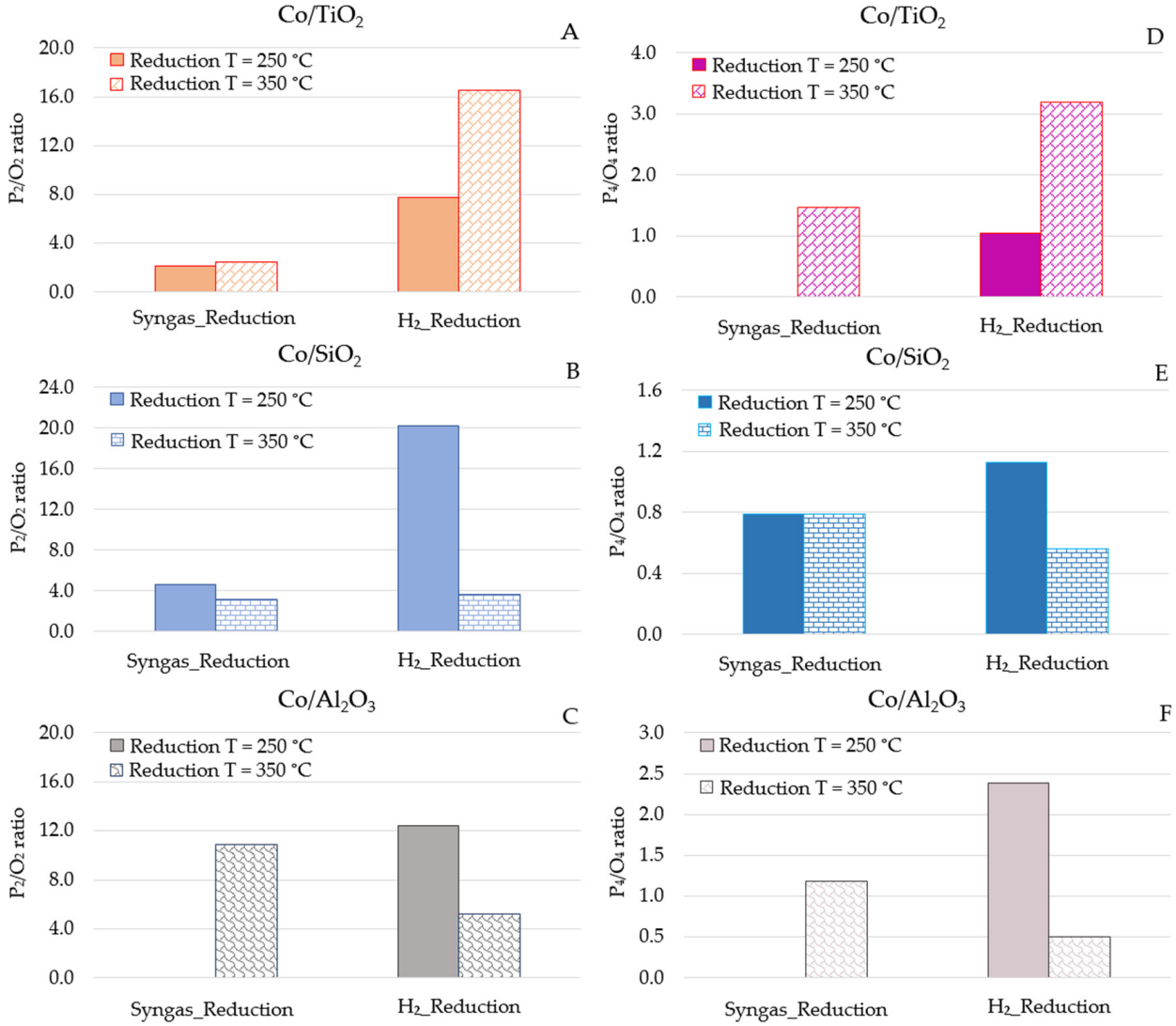

Figure 9. Paraffin to olefin ratio as a function of reducing agent and temperature: (**A**) P_2/O_2 for Co/TiO_2, (**B**) P_2/O_2 for Co/SiO_2, (**C**) P_2/O_2 for Co/Al_2O_3, (**D**) P_4/O_4 for Co/TiO_2, (**E**) P_4/O_4 for Co/SiO_2, and (**F**) P_4/O_4 for Co/Al_2O_3. Reaction conditions: 20 bar, 60 mL/min, and 210 °C. P_2/O_2 refers to the ratio of ethane/ethylene; P_4/O_4 refers to the ratio butane/butene.

The Co/SiO_2 catalyst with the highest surface area and lowest particle size (Table 1) was the most active catalyst when it reduced in H_2 at 250 °C (see Figure 4B). The high surface area of SiO_2-support and the lower metal–support interaction enhanced the reducibility and the dispersion of the metal. Our previous research [27] reported that the oxidised Co/SiO_2 catalyst, in H_2 at 250 °C, formed a multiphase of CoO–Co/SiO_2, and this CoO–Co interface promoted the CO dissociation and secondary olefin hydrogenation reactions, thus leading to a higher FT reaction rate [27].

Compared with SiO_2- and Al_2O_3-supported catalysts, the TiO_2-supported catalyst presented the highest CO reaction rates, when reduced either in H_2 or syngas at all temperatures except for the H_2-reduction at 250 °C. The lower surface area, observed via BET (Table 1) for the TiO_2-supported catalyst, promoted the agglomeration of the Co_3O_4 as larger Co_3O_4 particles, which might have increased their reducibility, and in consequence enhanced their catalytic activity. The low activity over the Al_2O_3-supported catalyst with the biggest Co_3O_4 particles (XRD: 33.0 nm in Table 1) must be related to the strong metal-support interaction (see Figure 3) and low metal dispersion due to the large cobalt particles (Table 1). For further discussion, please refer to Section 4.

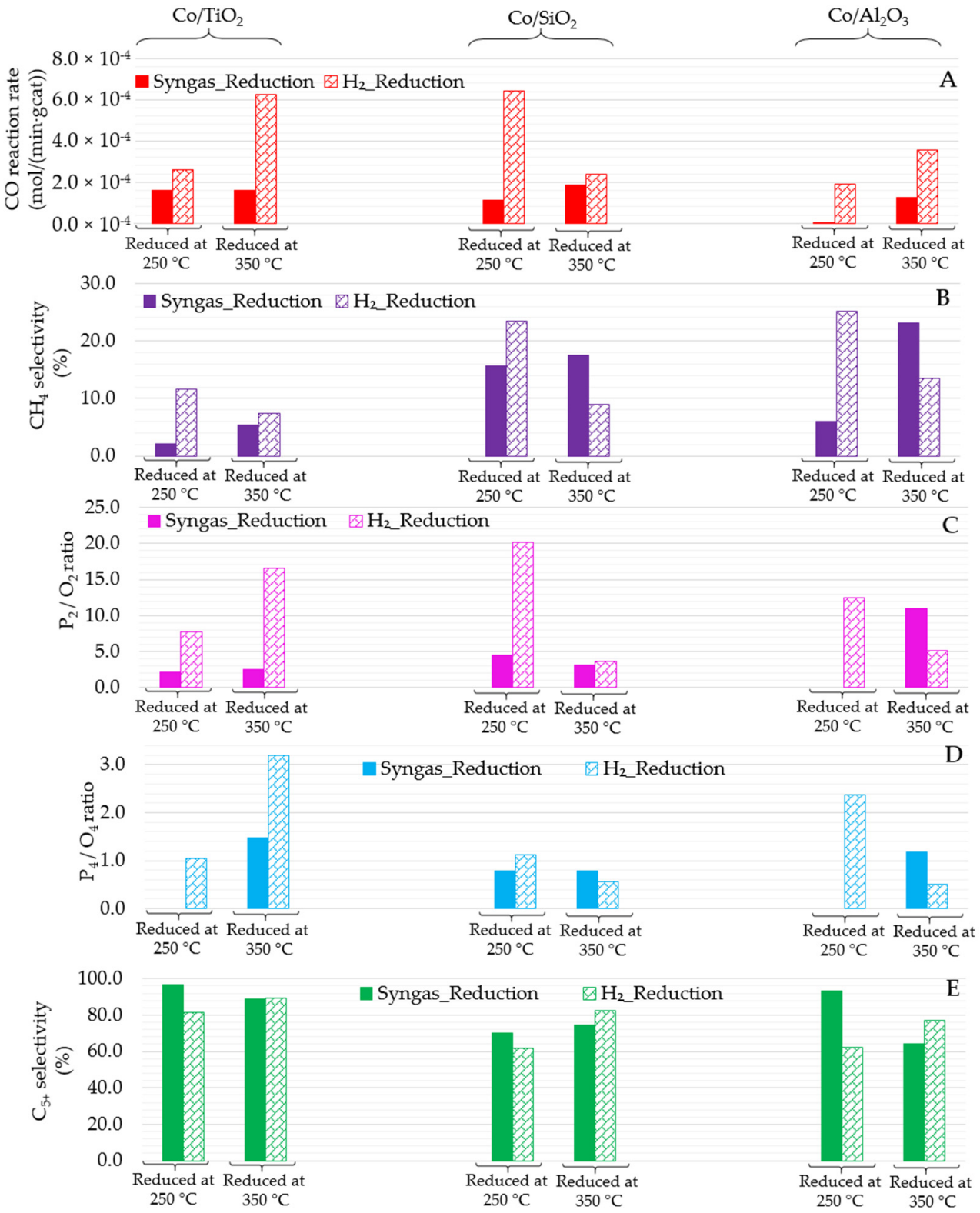

Figure 10. CO reaction rate and product selectivity as a function of reducing agent and temperature: (**A**) CO reaction rate, (**B**) CH_4 selectivity, (**C**) P_2/O_2 ratio, (**D**) P_4/O_4 ratio, and (**E**) C_{5+} selectivity. Reaction conditions: 20 bar, 60 mL/min, and 210 °C. P_2/O_2 refers to the ratio of ethane/ethylene; P_4/O_4 refers to the ratio butane/butene.

The CO reaction rates were found to be higher at a higher reduction temperature (350 °C) for all the samples, except for the syngas pre-treated TiO_2-supported sample and H_2-pre-treated SiO_2-supported sample. The SiO_2-supported catalyst showed higher

reaction rates at 250 °C compared to 350 °C (see Figure 4B). Our previous work over the SiO_2 sample demonstrated the effect of Co–CoO bonding promoting the FT reaction, thus leading to a higher FT reaction rate at a lower reduction temperature (250 °C), when the CoO density is higher than the density observed at 350 °C [27].

3.2.2. Product Formation Rate

The overall product formation rate as a function of temperature is illustrated in Figures 5 and 6. Changing the reduction medium from H_2 to syngas led to a complete change in the formation of products. A noticeable effect was the lower CH_4 formation rate observed for all the samples treated with syngas compared to H_2, excluding the SiO_2-supported catalyst treated with syngas at 350 °C. Co/TiO_2 showed the lowest CH_4 formation rate followed by Co/SiO_2 and then Co/Al_2O_3, at all reduction temperatures (see Figure 5). Another observation is that the CH_4 formation rate was higher for the syngas-treated samples at 350 °C, whereas for the H_2-treated samples, higher CH_4 formation rates were observed at 250 °C, except for the catalyst supported on SiO_2.

For long chain hydrocarbons (C_{5+}), higher formation rates were observed over the H_2-treated samples compared to the catalysts reduced in syngas (see Figure 6) due to lower CO reaction rates. Figure 6 shows that: (1) for H_2 reduction, higher C_{5+} formation rates were achieved at a higher reduction temperature for both TiO_2- and Al_2O_3-supported catalysts, while the higher C_{5+} formation rates were obtained at a lower reduction temperature for the SiO_2-supported catalysts; (2) for syngas reduction, higher C_{5+} formation rates were observed at a higher reduction temperature for both Al_2O_3- and SiO_2-supported catalysts, while there was only a slight difference between the C_{5+} formation rates at the reduction temperatures of 250 and 350 °C for the catalyst supported by TiO_2.

3.2.3. Product Selectivity

The effect of syngas or H_2 pre-treatment on the selectivity of the model cobalt catalysts as a function of temperatures is shown in Figures 7 and 8. All syngas-treated samples showed better selectivity (low CH_4, high C_{5+}) compared to H_2-reduced samples when reduced at a lower temperature, 250 °C. Increasing the syngas reduction temperature increased the CH_4 selectivity and decreased C_{5+} selectivity, whereas for the H_2-treated samples, an increase in the reduction temperature decreased the CH_4 selectivity and increased C_{5+} selectivity for all the three catalysts (Figure 8B). An increase in the reduction temperatures caused a slight increase in the selectivity of long chain hydrocarbons.

3.2.4. Paraffin to Olefin (P/O) Ratio

P/O ratio is a very important factor that reflects the selectivity of the paraffin (P) and olefin (O) products—a higher P/O ratio represents the products that are more paraffinic and a lower value indicates a higher selectivity to olefinic products. P_n/O_n represents the parafin to olefin ratio with carbon number n. In the current work, the ratios of P_2/O_2 (ethane/ethylene) and P_4/O_4 (butane/butene) are reported in Figure 9 for the catalysts either reduced by syngas or H_2 at different reduction temperatures. For the Co/TiO_2 catalyst, pre-treatment with syngas (at both 250 and 350 °C) produced more olefins than paraffins compared to the H_2 pre-treatment (low P/O ratios). For Co/SiO_2, similar results as for the Co/TiO_2 catalyst—lower P/O ratios were obtained for syngas-reduced catalysts compared to H_2 reduction at 250 °C. However, syngas pre-treatment at 350 °C produced more paraffin products over the Co/Al_2O_3 catalyst compared to H_2 pre-treatment at a similar reduction temperature.

4. Discussion and Implications

With the aim to understand the reaction pathways observed with different pre-treatment agents at different reduction temperatures, we replotted some of the data reported in Figures 4–9 in order to highlight the important findings of this work—the results are shown in Figure 10. The syngas-treated catalysts afforded a lower CO reaction rate

compared to H_2-treated samples (Figure 10A). This could be attributed to the lower Co site density caused by incomplete reduction of Co_3O_4 to metallic Co^0. Metallic Co^0 is known to be the active phase for the conversion of syngas to hydrocarbon products [20]; therefore, the lower the Co^0 density, the lower the CO hydrogenation activity. Our findings are in line with Gnanamani et al. [28] who reported that cobalt catalysts do not reduce completely under syngas treatment.

Catalyst pre-treatment is a way to transform cobalt oxides to active sites. For H_2 reduction, cobalt oxides are reduced to metallic Co^0; in the meantime, there is still some cobalt oxides (Co_3O_4 and/or CoO) left due to partial reduction depending on the reduction temperature or the extent of metal–support interactions. For syngas (a mixture of H_2/CO) reduction, the presence of CO in the mixture can also react with the cobalt oxides to form cobalt carbides (Co_xC), which has been confirmed by Peacock et al. [29] and Claeys et al. [30] using the in situ magnetometer. In addition, the Boudouard reaction ($2CO = CO_2 + C$) may occur when the operating temperature is high. Figure 11 lists the possible cobalt phases after cobalt catalyst reduction under different atmospheres.

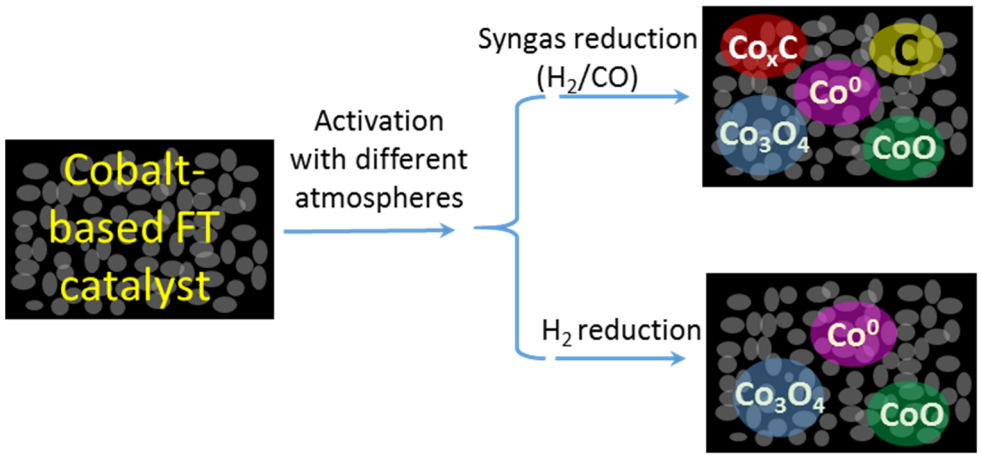

Figure 11. Cobalt phases during pretreatment of the cobalt-based FT catalyst.

From our experimental data (see Figure 10B–D), with syngas reduction at 250 °C, all the three catalysts had a much lower CH_4 selectivity and lower P/O ratio compared with the catalysts treated with H_2 at 250 °C, which indicates that the reactions of CO hydrogenation to paraffins were suppressed during the low temperature syngas reduction. These experimental results may provide evidence that the Co_2C phase promotes the formation of olefins by suppressing the olefin hydrogenation reaction. Furthermore, the existence of the metallic Co-hcp phase, obtained from further reduction of cobalt via the Co_xC intermediate, could catalyse the FT chain growth reaction by converting syngas to light olefins, which in turn react to form longer chain hydrocarbons for syngas-treated catalysts reduced at 250 °C. This reaction path is not the dominant mechanism for H_2-reduced catalysts at these reduction temperatures. On the basis of our results, we hypothesised that cobalt in association with the cobalt carbides enhances the production of higher hydrocarbons. Jiao et al. [31] and Gnanamani et al. [28] both supported this hypothesis in that they both suggested that Co_2C contributes to the selectivity of light olefin products and alcohol formation via a CO insertion mechanism. In addition, Jalama et al. [18] reported a higher olefin to paraffin ratio for the samples pre-treated in syngas than in H_2, which was attributed to the presence of the Co_2C phase.

The large shift in product selectivity by changing the activation conditions (as shown in Figures 5–9) led us to believe that the method of activation of cobalt as well as the corresponding temperature play vital roles in the subsequent hydrogenation of CO. A higher reduction temperature was found to increase the selectivity of C_1 in detriment to all other hydrocarbons (Figure 10), when syngas was used as a reducing agent. When reducing

at 350 °C, the Boudouard reaction may occur, and the carbonaceous deposits on the surface could act as methanation sites and decrease the number of Co active sites available for FTS. Findings over these catalysts suggest that carburisation and carbon deposits are feasible under syngas reduction, and that this may cause an increase in both the C_{5+} selectivity or CH_4 selectivity depending on the amount of surface carbon available. Our findings are in line with Lee et al. [32], who reported that surface carbonaceous deposits can exist in two forms, namely, active carbon or graphitic carbon, and that the active carbon can hydrogenate to methane under normal FT conditions.

In the case of H_2 pre-treated samples, an increase in the reduction temperature from 250 to 350 °C led to the production of higher hydrocarbons. These results demonstrate that C_{5+} hydrocarbon formation is a function of temperature and that a high reduction temperature is associated with a higher reducibility of Co_3O_4 to Co^0; therefore, it can be deduced that Co^0 is selective to the production of C_{5+} hydrocarbons.

This study also reflects on the effect of support properties on the performance of cobalt catalysts under different pre-treatment conditions. The catalyst supported on TiO_2 exhibited the highest selectivity towards liquid products with the lowest CH_4 selectivity when treated in both H_2 and syngas. This can be attributed to the higher Co site density observed via TEM (Figure 1A) and a higher reducibility, as established by the TPR profile in Figure 3, due to weaker metal interactions. On the other hand, Al_2O_3 showed the least activity (Figure 4) when both syngas and H_2 were used as a pre-treatment feed, due to (1) the strong metal–support interaction, resulting in lower reducibility, as observed via TPR, and (2) the lower metal dispersion, observed via TEM, caused by the larger Co_3O_4 particles that formed in the large alumina pores, observed via TEM, XRD, and BET (see Table 1). In the case of the SiO_2-support, the TPR reduction profile resembled that of the TiO_2 support, suggesting that the SiO_2 support is also weakly bonded to the Co metal. However, the Co/SiO_2 catalyst showed a different reactivity to that of TiO_2, which may have been due to a large surface area and a lower metal dispersion than the catalyst supported on TiO_2 (see Figure 1C and Table 1).

The support identity therefore plays a major role in the performance of the catalyst. Two parameters seem to determine the catalytic activity of the Co_3O_4 nanoparticles: (1) the Co particle size, which is influenced by the structure of the support, and (2) the extent of the metal–support interaction, metal–metal oxide interaction, and the metal–metal carbite interaction, which determines the specific nature of the active sites and their intrinsic catalytic activity.

5. Conclusions

The purpose of this study is to show the advantages of using syngas as a reducing agent for Co-FTS catalysts. To this end, we demonstrated the effect of the pre-treatment conditions by comparing the activity and product selectivity of the catalysts treated with syngas or H_2 at different temperatures. A lower CH_4 selectivity, higher C_{5+} selectivity, and lower P/O ratio were observed for the catalysts treated with syngas at 250 °C compared to the catalysts reduced either with H_2- at 250 °C or syngas at 350 °C. The formation of the Co_xC phase during the reduction in syngas may either: (1) act as an active site for the production of lower olefins or (2) suppress the hydrogenation reaction. On the basis of the experimental results, we hypothesised that there may be synergy between Co^0 and Co_xC to convert CO and H_2 to long chain hydrocarbons.

Author Contributions: Conceptualisation, Y.Y. and X.L.; methodology, N.C.S., Y.Y. and X.L.; software, N.C.S.; validation, Y.Y., X.L. and D.H.; formal analysis, N.C.S.; investigation, N.C.S.; resources, Y.Y., D.H. and X.L.; writing—original draft preparation, N.C.S.; writing—review and editing, Y.Y. and D.H.; supervision, Y.Y., X.L. and D.H.; project administration, Y.Y. and X.L. All authors have read and agreed to the published version of the manuscript.

Funding: This research was funded by the South Africa's National Research Foundation (Grant number: NRF UID 95445 and 117793).

Institutional Review Board Statement: Not applicable.

Informed Consent Statement: Not applicable.

Data Availability Statement: Data presented in this article is available from the corresponding author on reasonable request.

Acknowledgments: The authors are grateful for the support received from the University of South Africa (UNISA) and the South Africa's National Research Foundation.

Conflicts of Interest: The authors declare no conflict of interest. The funders had no role in the design of the study; in the collection, analyses, or interpretation of data; in the writing of the manuscript; or in the decision to publish the results.

References

1. Kliewer, C.E.; Soled, S.L.; Kiss, G. Morphological transformations during Fischer-Tropsch synthesis on a titania-supported cobalt catalyst. *Catal. Today* **2019**, *323*, 233–256. [CrossRef]
2. Chen, P.P.; Liu, J.X.; Li, W.X. Carbon monoxide activation on cobalt carbide for Fischer–Tropsch synthesis from First-Principles theory. *ACS Catal.* **2019**, *9*, 8093–8103. [CrossRef]
3. Dalai, A.K.; Davis, B.H. Fischer–Tropsch synthesis: A review of water effects on the performances of unsupported and supported Co catalysts. *Appl. Catal. A Gen.* **2008**, *348*, 1–15. [CrossRef]
4. Voß, M.; Borgmann, D.; Wedler, G. Characterization of alumina, silica, and titania supported cobalt catalysts. *J. Catal.* **2002**, *212*, 10–21. [CrossRef]
5. Lyu, S.; Wang, L.; Zhang, J.; Liu, C.; Sun, J.; Peng, B.; Wang, Y.; Rappé, K.G.; Zhang, Y.; Li, J.; et al. Role of active phase in Fischer–Tropsch synthesis: Experimental evidence of CO activation over single-phase cobalt catalysts. *ACS Catal.* **2018**, *8*, 7787–7798. [CrossRef]
6. Borg, Ø.; Dietzel, P.D.C.; Spjelkavik, A.I.; Tveten, E.Z.; Walmsley, J.C.; Diplas, S.; Eri, S.; Holmen, A.; Rytter, E. Fischer–Tropsch synthesis: Cobalt particle size and support effects on intrinsic activity and product distribution. *J. Catal.* **2008**, *259*, 161–164. [CrossRef]
7. Rytter, E.; Holmen, A. On the support in cobalt Fischer–Tropsch synthesis—Emphasis on alumina and aluminates. *Catal. Today* **2016**, *275*, 11–19. [CrossRef]
8. Khodakov, A.Y.; Griboval-Constant, A.; Bechara, R.; Zholobenko, V.L. Pore size effects in Fischer Tropsch synthesis over cobalt-supported mesoporous silicas. *J. Catal.* **2002**, *206*, 230–241. [CrossRef]
9. Song, D.; Li, J. Effect of catalyst pore size on the catalytic performance of silica supported cobalt Fischer–Tropsch catalysts. *J. Mol. Catal. A Chem.* **2006**, *247*, 206–212. [CrossRef]
10. Borg, Ø.; Eri, S.; Blekkan, E.A.; Storsæter, S.; Wigum, H.; Rytter, E.; Holmen, A. Fischer–Tropsch synthesis over γ-alumina-supported cobalt catalysts: Effect of support variables. *J. Catal.* **2007**, *248*, 89–100. [CrossRef]
11. Jacobs, G.; Das, T.K.; Zhang, Y.; Li, J.; Racoillet, G.; Davis, B.H. Fischer–Tropsch synthesis: Support, loading, and promoter effects on the reducibility of cobalt catalysts. *Appl. Catal. A Gen.* **2002**, *233*, 263–281. [CrossRef]
12. Zhang, J.; Chen, J.; Ren, J.; Li, Y.; Sun, Y. Support effect of Co/Al_2O_3 catalysts for Fischer–Tropsch synthesis. *Fuel* **2003**, *82*, 581–586. [CrossRef]
13. Soled, S.L.; Iglesia, E.; Fiato, R.A.; Baumgartner, J.E.; Vroman, H.; Miseo, S. Control of metal dispersion and structure by changes in the solid-state chemistry of supported cobalt Fischer–Tropsch catalysts. *Top. Catal.* **2003**, *26*, 101–109. [CrossRef]
14. Vosoughi, V.; Badoga, S.; Dalai, A.K.; Abatzoglou, N. Effect of pretreatment on physicochemical properties and performance of multiwalled carbon nanotube supported cobalt catalyst for Fischer–Tropsch Synthesis. *Ind. Eng. Chem. Res.* **2016**, *55*, 6049–6059. [CrossRef]
15. Mehrbod, M.; Martinelli, M.; Martino, A.G.; Cronauer, D.C.; Kropf, A.J.; Marshall, C.L.; Jacobs, G. Fischer-Tropsch synthesis: Direct cobalt nitrate reduction of promoted Co/TiO_2 catalysts. *Fuel* **2019**, *245*, 488–504. [CrossRef]
16. De la Peña O'Shea, V.A.; Campos-Martin, J.M.; Fierro, J.L.G. Strong enhancement of the Fischer–Tropsch synthesis on a Co/SiO_2 catalyst activate in syngas mixture. *Catal. Comm.* **2004**, *5*, 635–638. [CrossRef]
17. Tsubaki, N.; Sun, S.; Fujimoto, K. Different functions of the noble metals added to cobalt catalysts for Fischer–Tropsch synthesis. *J. Catal.* **2001**, *199*, 236–246. [CrossRef]
18. Jalama, K.; Kabuba, J.; Xiong, H.; Jewell, L.L. Co/TiO_2 Fischer–Tropsch catalyst activation by synthesis gas. *Catal. Comm.* **2012**, *17*, 154–159. [CrossRef]
19. Dai, Y.; Zhao, Y.; Lin, T.; Li, S.; Yu, F.; An, Y.; Wang, X.; Xiao, K.; Sun, F.; Jiang, Z.; et al. Particle size effects of cobalt carbide for Fischer–Tropsch to olefins. *ACS Catal.* **2018**, *9*, 798–809. [CrossRef]
20. Claeys, M.; Dry, M.E.; van Steen, E.; van Berge, P.J.; Booyens, S.; Crous, R.; van Helden, P.; Labuschagne, J.; Moodley, D.J.; Saib, A.M. Impact of process conditions on the sintering behavior of an alumina-supported cobalt Fischer–Tropsch catalyst studied with an in-situ magnetometer. *ACS Catal.* **2015**, *5*, 841–852. [CrossRef]
21. Yang, J.; Jacobs, G.; Jermwongratanachai, T.; Anders, D.C.; Burtron, H. Fischer–Tropsch synthesis: Impact of H_2 or CO activation on methane selectivity. *Catal. Lett.* **2014**, *144*, 123–132. [CrossRef]

22. Li, J.; Xu, L.; Keogh, R.; Davis, B. Fischer–Tropsch synthesis: Effect of CO pretreatment on a ruthenium promoted Co/TiO_2. *Catal. Lett.* **2000**, *70*, 127–130. [CrossRef]
23. Pei, Y.P.; Liu, J.X.; Zhao, Y.H.; Ding, Y.J.; Liu, T.; Dong, W.D.; Zhu, H.J.; Su, H.Y.; Yan, L.; Li, J.L.; et al. High alcohols synthesis via Fischer–Tropsch reaction at cobalt metal/carbide interface. *ACS Catal.* **2015**, *5*, 3620–3624. [CrossRef]
24. Chen, W.; Kimpel, T.F.; Song, Y.; Chiang, F.K.; Zijlstra, B.; Pestman, R.; Wang, P.; Hensen, E.J. Influence of carbon deposits on the cobalt-catalyzed Fischer–Tropsch reaction: Evidence of a two-site reaction model. *ACS Catal.* **2018**, *8*, 1580–1590. [CrossRef] [PubMed]
25. Fischer, N.; Clapham, B.; Feltes, T.; Claeys, M. Cobalt-based Fischer–Tropsch activity and selectivity as a function of crystallite size and water partial pressure. *ACS Catal.* **2015**, *5*, 113–121. [CrossRef]
26. Tucker, C.L.; van Steen, E. Activity and selectivity of a cobalt-based Fischer-Tropsch catalyst operating at high conversion for once-through biomass-to-liquid operation. *Catal. Today* **2020**, *342*, 115–123. [CrossRef]
27. Shiba, N.C.; Yao, Y.; Forbes, R.P.; Okoye-Chine, C.G.; Liu, X.; Hildebrandt, D. Role of CoO-Co nanoparticles supported on SiO_2 in Fischer-Tropsch synthesis: Evidence for enhanced CO dissociation and olefin hydrogenation. *Fuel Proc. Technol.* **2021**, *216*, 106781. [CrossRef]
28. Gnanamani, M.K.; Jacobs, G.; Keogh, R.A.; Shafer, W.D.; Sparks, D.E.; Hopps, S.D.; Thomas, G.A.; Davis, B.H. Fischer-Tropsch synthesis: Effect of pretreatment conditions of cobalt on activity and selectivity for hydrogenation of carbon dioxide. *Appl. Catal. A Gen.* **2015**, *499*, 39–46. [CrossRef]
29. Peacock, M.; Purves, R.; Ojeda, M.; Ferguson, E.; Paterson, J. In situ diffraction of Fischer-Tropsch catalysts: Cobalt reduction and carbide formation. *ChemCatChem* **2017**, *9*, 3463–3469. [CrossRef]
30. Claeys, M.; Dry, M.E.; van Steen, E.; Du Plessis, E.; Van Berge, P.J.; Saib, A.M.; Moodley, D.J. In situ magnetometer study on the formation and stability of cobalt carbide in Fischer–Tropsch synthesis. *J. Catal.* **2014**, *318*, 193–202. [CrossRef]
31. Jiao, F.; Li, J.; Pan, X.; Xiao, J.; Li, H.; Ma, H.; Wei, M.; Pan, Y.; Zhou, Z.; Li, M.; et al. Selective conversion of syngas to light olefins. *Science* **2016**, *351*, 1065–1068. [CrossRef] [PubMed]
32. Lee, D.; Lee, J.; Ihm, S. Effect of carbon deposits on carbon monoxide hydrogenation over alumina-supported cobalt catalyst. *Appl. Catal.* **1988**, *36*, 199–207. [CrossRef]